fibers

Article

Thermal, Optical, and Emission Traits of SM^{3+}-Ion-Doped Fluoride/Chloride/Oxide Glass for Red/Orange Laser Fiber Applications

Bozena Burtan-Gwizdala [1], Jan Cisowski [1], Radoslaw Lisiecki [2], Kinga J. Kowalska [3], Bozena Jarzabek [4], Natalia Nosidlak [1], Manuela Reben [3], Ali M. Alshehri [5], Khalid I. Hussein [6,*] and El Sayed Yousef [5]

[1] Institute of Physics, Cracow University of Technology, ul. Pochorazych 1, 30-084 Cracow, Poland; burtan_bozena@wp.pl (B.B.-G.); bobo55555@wp.pl (J.C.); natalia.nosidlak@gmail.com (N.N.)
[2] Institute of Low Temperatures and Structure Research, Polish Academy of Sciences, ul. Okolna 2, 50-950 Wroclaw, Poland; r.lisiecki@int.pan.wroc.pl
[3] Faculty of Materials Science and Ceramics, AGH-University of Krakow, al. A. Mickiewicza 30, 30-059 Cracow, Poland; kjkowalska@agh.edu.pl (K.J.K.); manuelar@agh.edu.pl (M.R.)
[4] Centre for Polymer and Carbon Materials, Polish Academy of Sciences, ul. Marii Curie-Skłodowskiej 34, 41-819 Zabrze, Poland; bozena.jarzabek@cmpw-pan.edu.pl
[5] Department of Physics, Faculty of Science, King Khalid University, P.O. Box 9004, Abha 61413, Saudi Arabia; amshehri@kku.edu.sa (A.M.A.); ayousf@kku.edu.sa (E.S.Y.)
[6] Department of Radiological Sciences, College of Applied Medical Sciences, King Khalid University, Abha 61421, Saudi Arabia
* Correspondence: kirahim@kku.edu.sa

Abstract: This study examined spectroscopic, thermal, and other qualities, such as the lasing parameters, of Sm^{3+}-doped glass with the composition $40P_2O_5$–30ZnO–20LiCl–$10BaF_2$. The ellipsometric data were used in a Sellmeier dispersion relation to estimate the refractive index values of the glasses investigated. The measured absorption spectra of the doped glass reveal the presence of various absorption bands assigned to transitions from the $^6H_{5/2}$ ground state attributed to Sm^{3+}-ion-excited states. We studied the decay of the $^4G_{5/2}$ level of the Sm^{3+} ions in the doped glass by analyzing its absorption and emission fluorescence spectra. The Judd–Ofelt hypothesis allowed us to determine that the quantum efficiency of the $^4G_{5/2}$–$^6H_{7/2}$ transition is high: 96% and 97% for glass doped with 4.05×10^{19} ions/cm^{-3} and 11×10^{19} ions/cm^{-3}, respectively. Furthermore, this glass exhibits efficient red/orange enhanced spontaneous emission that matches the excitation band of the photosensitizer material used in medical applications.

Keywords: thermal stability; absorption cross-section; emission spectra; refractive index; spectroscopic quality parameters; quantum efficiency

check for updates

Citation: Burtan-Gwizdala, B.; Cisowski, J.; Lisiecki, R.; Kowalska, K.J.; Jarzabek, B.; Nosidlak, N.; Reben, M.; Alshehri, A.M.; Hussein, K.I.; Yousef, E.S. Thermal, Optical, and Emission Traits of SM^{3+}-Ion-Doped Fluoride/Chloride/Oxide Glass for Red/Orange Laser Fiber Applications. *Fibers* **2024**, *12*, 100. https://doi.org/10.3390/fib12110100

Academic Editor: Giancarlo C. Righini

Received: 22 July 2024
Revised: 14 October 2024
Accepted: 11 November 2024
Published: 15 November 2024

1. Introduction

Phosphate glasses possess high thermal stability, relatively low melting temperatures, and unique optical properties, along with a broad range of transparency in the UV-VIS spectral range; however, they have a low refractive index [1]. Therefore, phosphate glasses doped with rare-earth (RE) ions are widely studied for their applications in waveguides, optical detectors, fiber optic amplifiers, and lasers [2]. The addition of various fluorides to RE-ion-doped phosphate glasses enables the creation of host matrices that combine the significant optical properties of fluoride glasses and the high stability of phosphate glasses. Oxides increase the mechanical resistance and thermal stability of the glasses, while low-frequency fluorides reduce the nonradiative decay losses caused by multifamily relaxation [3], improve the quantum efficiency and lifetimes of rare-earth ions' luminescence, and act as flux agents that reduce the melting temperature of the glasses. When samarium ions are doped into fluorophosphate glass, the resulting glass exhibits distinctive optical behavior due to its emissions in the UV–visible region through various emission channels from the $^4G_{5/2}$ level of Sm^{3+} ions [4]. Samarium ions (Sm^{3+}) are regarded as excellent luminescent centers among the rare-earth (RE^{3+}) ions due to their strong emissions at longer wavelengths in the red/orange region. The strong luminescence in the red/orange region, as well as the high quantum efficiency value of Sm^{3+}-doped P_2O_5–Na_2O–BaO–Al_2O_3 glasses, makes them a potential candidate for laser emission [5].

This characteristic makes them highly suitable for applications in solid-state lasers, LEDs, and display devices. Additionally, the lowest emitting level of Sm^{3+} ions, $^4G_{5/2}$, exhibits high quantum efficiency and various quenching emission channels [6,7]. The $^4f_5$ configuration of samarium ions with strong orange-red fluorescence in the visible region is used in underwater communications, color displays, visible semiconductor lasers [8–10], and phosphors for white light-emitting diodes (LEDs) [11,12]. Although extensive research has been conducted on phosphate glasses doped with Sm^{3+} ions [13–16], there is still a need to explore new and advanced compositions of phosphate glass due to their potential applications.

In [17], the researchers confirmed the formation of defects and the conversion of Sm^{3+} into Sm^{2+} ions in Sm-doped fluorophosphate glasses exposed to X-ray irradiation. Additionally, Hamdy et al. [18] synthesized compositions containing 20, 30, and 50 mol% NaF, AlF_3, and PF_5 doped with Sm^{3+} to investigate the impact of Sm^{3+} on optical transmission and photoluminescence (PL) spectroscopy. The authors of [19] discussed the influence of the chemical composition of [(45 − x) P_2O_5–10AlF_3–45 NaF x Sm_2O_3](where x equal 0 to 1 mol%) glasses on their optical properties, mainly their linear and non-linear parameters. The study performed by [20] focused on examining the thermal, structural, and luminescent characteristics of sodium barium metaphosphate glasses doped with Sm^{3+}. Samarium-doped fluoroaluminate and fluorophosphate glasses studied by Chicilo et al. [21] proved to be excellent candidates for high-resolution, large-dynamic-range microbeam radiation therapy (MRT) dosimetry. It is worth noting that Sm^{3+} ions are ideal for doping because their excited energy level $^4G_{5/2}$ has a high quantum efficiency with various quenching emission channels. It emits strong reddish-orange light and possesses sufficient energy to initiate photodynamic reactions. Recently, lasers with excellent directivity and high intensity, as well as LEDs with relatively narrow spectral bandwidths and high fluence rates, have been specifically developed for photodynamic therapy (PDT) treatments. However, scattered or misdirected light from the target area can unintentionally expose large areas of normal tissue to high power densities, potentially leading to side effects such as inflammation, pain, swelling, burns, and scarring. While LEDs can be integrated with optical fibers, their low coupling efficiency limits their use. Additionally, their narrow excitation spectrum restricts the use of multiple photosensitizers, reducing the efficiency of therapy. Amplified spontaneous emission (ASE) fluorescence produced in rare-earth (RE) ion-doped glass channel waveguides offers a broadened bandwidth that can be tuned by adjusting the RE ion concentration and pumping power. This type of light source delivers sufficient intensity, excellent directivity, and high coupling efficiency, making it a promising option for use in photodynamic therapy (PDT) treatments [22].

A fluorophosphate glass channel waveguide produces amplified spontaneous emission (ASE) fluorescence with a broad width of 600–730 nm. This light source has excellent efficiency, strong intensity, and good directivity, thus making it an attractive option for use in photodynamic therapy (PDT) [22,23]. Red light in the 600–730 nm spectral band has 50–200% greater penetrating power than light in the 400–500 nm region, and it possesses more energy to initiate a photodynamic reaction that produces $^1O_2$ according to most tissue models [22]. A diverse range of light sources, both coherent and incoherent, have demonstrated their effectiveness in achieving anti-tumor effects in PDT for various superficial and interstitial treatment sites [24–26]. Thus, in this paper, we have focused on the lasing parameters of Sm^{3+}-doped fluorophosphate glasses as a candidate light source for photodynamic therapy (PDT). In the glass compositions, we included BaF_2 ions as network modifier ions with a low field strength and ZnO to improve the mechanical strength, chemical durability, and hygroscopic nature, which, in turn alter, the optical, electrical, and magnetic properties of phosphate glasses.

2. The Experimental Section

The composition of the glasses was chosen as $40P_2O_5$–30ZnO–20LiCl–$10BaF_2$ with different concentrations of Sm^{3+} ions: sample 1 (SM1) at 4.05×10^{19} cm^{-3} and sample 2 (SM2) at 11×10^{19} cm^{-3}. The following chemicals were used for batch production: phosphorus oxide (P_2O_5), zinc oxide (ZnO), lithium chloride (LiCl), barium fluoride (BaF_2), and samarium oxide (Sm_2O_3). All of the raw materials were carefully mixed. The fluorophosphate glasses were obtained by melting 50 g batches in a gold crucible in an electric furnace at a temperature of 850°C in an air atmosphere [27]. The densities of the glasses studied were determined using Archimedes' method (Table 1).

Table 1. Volume concentration (N), glass matrix composition (mol%), density, and refractive index at 633 nm.

Sample	Composition (mol%)	N (10^{19} cm^{-3})	Density (g/cm^3)	n
SM	$40P_2O_5$–30ZnO–20LiCl–$10BaF_2$	----	3.872	1.588
SM1	$40P_2O_5$–30ZnO–20LiCl–$10BaF_2$–XSm_2O_3	4.05	3.792	1.585
SM2	$40P_2O_5$–30ZnO–20LiCl–$10BaF_2$–YSm_2O_3	11.00	3.821	1.579

Their refractive indexes were determined with use of a Woollam M-2000 ellipsometer; the spectra were recorded in the 190–1700 nm spectral range. The transmittance and reflectance spectra were recorded using Jasco V-570 spectrophotometers [27]. Luminescence spectra were measured using the Optron Dong Woo fluorometer system [28]. The luminescence decay curves were measured following short-pulse excitation provided by an optical parametric oscillator with the third harmonic of a Nd YAG laser [29,30]. Changes in the thermal behavior of the $40P_2O_5$–30ZnO–20LiCl–$10BaF_2$ glasses were investigated with the DTA/DSC method using the PerkinElmer DTA-7 System.

Under a flowing air environment (80 mL min^{-1}), the glass samples were ground into powders with grain sizes of 0.1 to 0.3 mm and then heated in platinum crucibles at a rate of 10 °C min^{-1}.

Alumina oxide (Al_2O_3) was used as a reference material. Several thermal parameters characteristic of the glassy state have been established, i.e., the glass transformation temperature (T_g) and the glass crystallization temperature (T_c). Using the midpoint of the corresponding transformation phase as the glass conversion temperature (T_g) and the start and maximum of the glass crystallization peak as the parameters for the glass melting and solidification processes, we were able to obtain the glass heating and solidification temperatures.

While the midpoint of the corresponding transformation step was used to estimate the glass conversion temperature (T_g), the start (T_x) and maximum (T_c) of the glass crystallization peak were used to calculate the glass crystallization temperature.

The characteristic glass temperature values that appeared in DSC were determined using Proteus Thermal Analysis (Version 5.0.0.). The amorphous nature of the glasses studied was confirmed using the X-ray diffraction (XRD) method and a Philips X'Pert X-ray diffractometer with CuK_α radiation. All of the research was conducted at room temperature. The refractive index of the bulk glasses was investigated using transmission mode ellipsometric data. The ellipsometric results were registered in the range of 400–1700 nm, and n was modeled using the Sellmeier dispersion function. Therefore, the Sellmeier refractive index (n)'s normal dispersion, which was determined from our ellipsometric data collected as a function of the wavelength λ (see Equation (1)) [31,32], was fitted to the low-absorption region, which is 400–1700 nm.

$$n^2 = A + B_\lambda{}^2/(\lambda^2 - C^2) - D_\lambda{}^2 \quad (1)$$

where A, B, C, and D are the fitting parameters.

The refractive index dispersions of the glasses studied are quite similar to each other, as are the values of n measured at 633 nm (see Table 1). The addition of Sm_2O_3 to the glasses led to a decrease in the refractive index compared to the sample SM without a dopant.

It is worth mentioning that ellipsometry is not a direct method for determining the refractive index.

3. Results and Discussion

3.1. Thermal Analysis

The broad hump in the XRD profile shows the long-term structural instability (i.e., random atomic arrangements) of the glasses prepared (Figure 1). Therefore, based on XRD analysis of all the glasses, it can be found that they are amorphous. The differential scanning calorimetry (DSC) curves of all of the glasses studied showed distinct endothermic events associated with the glass transition T_g, as well as the melting point T_m. The exothermic event T_c associated with crystallization was observed. During heating, the glasses studied demonstrate several characteristic temperatures. The range of vitreous state transitions ($T_{g,endset} - T_{g,onset}$) decreases progressively when the Sm^{3+} ion concentration in the glass increases, although the transition temperature increases (Figure 2).

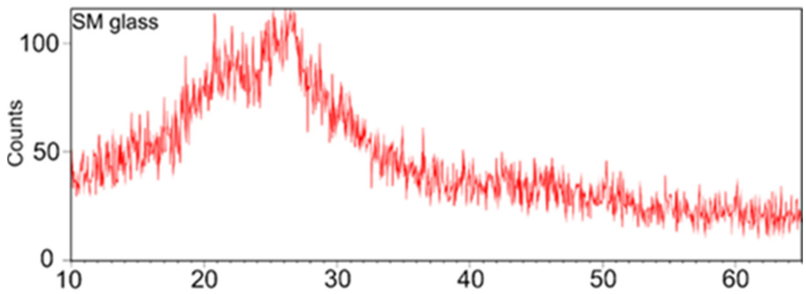

Figure 1. XRD pattern of the reference glass SM.

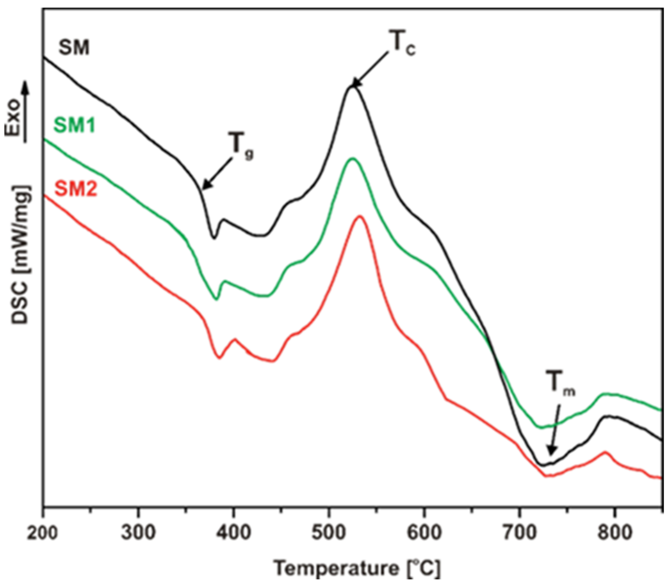

Figure 2. DSC curves of Sm^{3+}-doped fluorophosphate glasses.

The increase in T_g refers to structural changes in the glass network with increasing Sm^{3+}; furthermore, the narrowing of the transition range of the vitreous state (i.e., a reduction in the relaxation time) supports the theory of increased rigidity in the material's internal structure (Table 2). According to [33], this process occurs via the breaking of chemical bonds rather than the displacement of structural units when the time required for structural strain relaxation shortens, maintaining the network's continuity. To determine the thermal behavior of glasses, many parameters have been established, mainly considering the dependencies between values of characteristic temperatures. To evaluate the stability of the glass, the following parameters were utilized: the Hruby (K_H) = ($T_x - T_g$)/($T_m - T_x$) [34], the Weinberg (K_W) = ($T_x - T_g$)/T_m), the Lu and Liu (K_{LL}) = T_x/($T_g + T_m$)), and the Angell K_A = ($T_x - T_g$) parameters [35]. The resistance of the resulting material to crystallization is expressed by the term ($T_x - T_g$) in the suggested formula; a narrower gap indicates an increased tendency to crystallize. As the concentration of Sm^{3+} ions in the glasses increased, their K_A was in the 69–73 °C temperature range. Greater Sm^{3+} doping results in a higher KA value, increasing the glass's thermal stability.

Table 2. Thermal characteristics of Sm^{3+}-doped fluorophosphate glasses.

Glass ID	T_g	$T_{g\ range}$	T_x	T_c	T_m
SM	357	23	426	523	720
SM1	369	14	440	526	725
SM2	372	5	445	540	733

Abbreviations: T_g—glass transition temperature, T_x—endothermic onset of the maximum crystallization peak in glass; T_c—maximum crystallization peak in glass, T_m—endo thermic peak (glass melting temperature).

The stronger thermal stability of glass against devitrification on heating was further verified by the fact that the values of other thermal stability metrics, such as K_w, K_H, and K_{LL}, increased with larger Sm^{3+} concentrations. Not only can one infer a material's stability from all these variables but one can also infer its glass-forming ability, which is the ease with which a liquid vitrifies upon cooling. Table 3 shows that the stability and glass-forming ability of $40P_2O_5$–30ZnO–20LiCl–$10BaF_2$ glasses are enhanced when the Sm^{3+} ion concentration in their structure increases. Both Mawlud et al. and Mnjeet et al. [36,37] found similar correlations in their studies.

Table 3. Stability parameters of the Sm^{3+}-doped fluorophosphate glasses.

Glass ID	Hruby/K_H	Weinberg/K_W	Lu and Liu/K_{LL}	K_A
SM	0.234	0.095	0.395	69
SM1	0.249	0.097	0.402	71
SM2	0.253	0.099	0.403	73

Abbreviations: K_A—Angell parameter, K_H—Hruby parameter, K_W—Weinberg parameter, K_{LL}—Lu and Liu parameter.

3.2. Absorption and Excitation Spectra

The transmittance and reflectance spectra allowed us to calculate the dispersion of the absorption coefficient of the fluorophosphate glasses doped with the Sm^{3+} ions. The results are illustrated in Figures 3 and 4.

As shown in Figures 3 and 4, the absorption spectra of the Sm^{3+}-doped fluorophosphate glasses registered in the UV-VIS-NIR region showed 19 peaks. As can be seen in Figures 3 and 4, these peaks are caused by Sm^{3+} ions' transition from the $^6H_{5/2}$ ground state to various energy levels [38,39].

The absorption spectra allowed us to observe a large number of energy transitions of the samarium ions in the glass from the system P_2O_5–ZnO–LiCl–BaF_2. Above 450–500 nm, in the SM1 and SM2 glasses, one may find the high energy manifolds built from the ^4D, ^4G, ^4I, ^4L, and ^4M quartets and ^6P sextet terms. Because many $^{2S+1}L_J$ splitters overlap, the UV-VIS bands that are visible are less intense and difficult to identify. Shifts in the absorption edge towards the UV region are observed with an increasing Sm^{3+} ion content. However, the bands that formed in the near-infrared spectrum are more distinct and strongly differentiated. In the spectral range of 500–250 nm, there is a comparable effect; however, in contrast, intense absorption peaks at 402 nm occurred, and this band is associated with transitions ending in $^4M_{19/2}$, $^6P_{3/2}$, $^4L_{15/2}$, $^6P_{7/2}$, $^4D_{3/2}$, $^4D_{7/2}$, $^3P_{3/2}$, and $^4P_{5/2}$ closely spaced multiples.

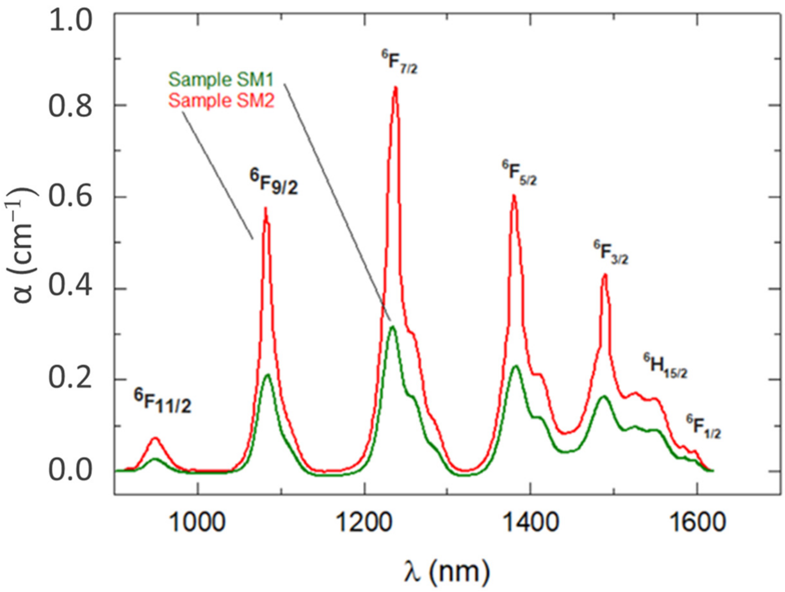

Figure 3. Absorption spectra of Sm^{3+}-doped fluorophosphate glass samples in the range of 800–1600 nm (NIR).

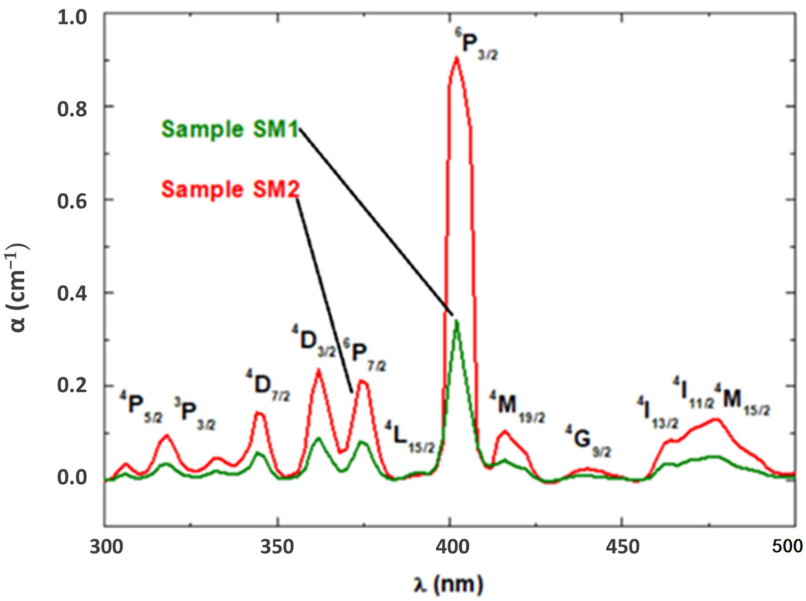

Figure 4. Absorption spectra of Sm^{3+}-doped fluorophosphate glass samples in the range of 300–500 nm (UV-VIS).

In addition, the absorption spectra of the glasses tested were supplemented by photoluminescent excitation spectra, which are shown in Figure 5.

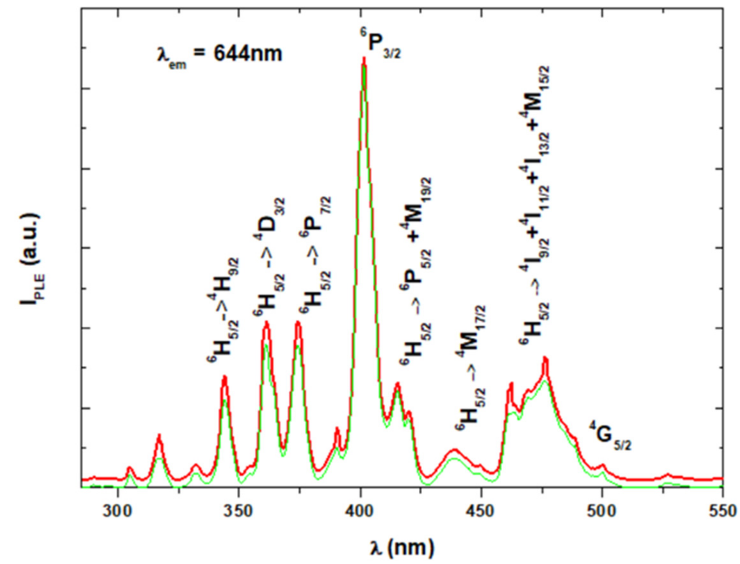

Figure 5. The absorption spectra of phosphate glasses doped with Sm^{3+} were observed at 644 nm in the photoluminescence excitation (PLE) mode.

Figure 6 shows the absorption cross-section (ACS) of the $^6H_{5/2} \rightarrow {}^6F_{7/2}$ transition, which is fundamental for samarium-doped fiber amplifiers. The ACS is defined as $\sigma_{abs} = \alpha/N$ and is easily obtained from the absorption spectra shown in Figure 3.

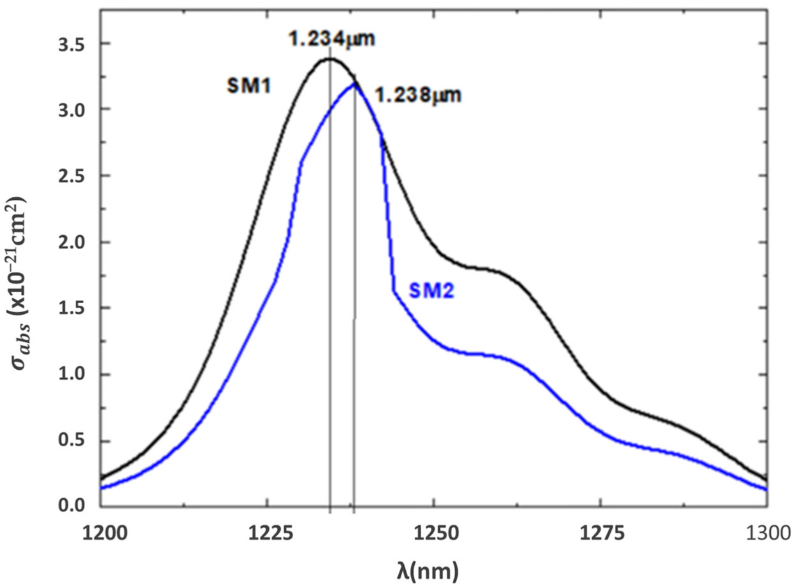

Figure 6. Absorption cross-section σ_{abs} (λ) of investigated glasses for $^6H_{5/2} \rightarrow {}^6F_{7/2}$ transition.

The most significant transitions of Sm^{3+} ions occur in the range of 1000–1300 nm, corresponding to the $^6H_{5/2} \rightarrow {}^6F_{9/2}$ and $^6H_{5/2} \rightarrow {}^6F_{7/2}$ transitions of Sm^{3+} ions (Figure 6).

Figure 7 presents the absorption cross-section (σ_{abs}) calculated for the SM1 and SM2 glasses, and the maximum value at 402 nm was $\sigma_{abs} = 17.0067 \times 10^{-21}$ cm^2 for SM2 and $\sigma_{abs} = 14.1206 \times 10^{-21}$ cm^2 for SM1.

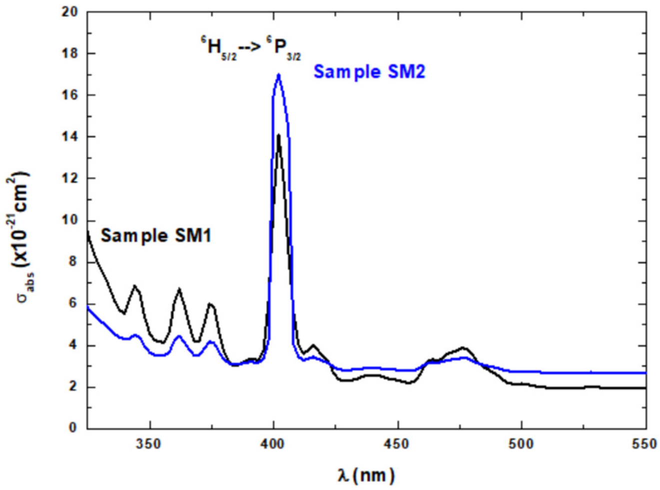

Figure 7. The calculated absorption cross-section (σ_{abs}) for the investigated glasses for the $^6H_{5/2} \rightarrow$ $^6P_{3/2}$ transition of Sm^{3+} ions.

3.3. Judd–Ofelt Analysis

Here, we analyzed the absorption data using the conventional Judd–Ofelt (J—O) theory (Figures 3 and 4). Numerical integration of suitable absorption bands, excluding the background absorption of the glass arrays, was used to establish the experimental oscillator strengths for transitions from the Sm^{3+} ions' ground level $^6H_{5/2}$ to subsequent excited levels.

Many intense transitions can be observed in the PLE spectrum (Figure 5), like those in the absorption spectra. In Table 4, the computed J–O parameters (Ω_2, Ω_4, and Ω_6) can be observed. Judd–Ofelt parameters are a useful tool for determining the radiative properties of Sm^{3+}-doped glasses, which are strongly dependent on the host matrix. The values of the J–O parameters obtained [40,41] are comparable to values found in other phosphate glasses doped with Sm^{3+} and show the same trend, namely $\Omega_4 > \Omega_6 > \Omega_2$ [42,43]. The values of Ω_4 and Ω_6 are associated with structural qualities like the viscosity and stiffness of the material, whereas the value of Ω_2 indicates the covalency of oxygen atoms and the asymmetry of the RE ion sites, according to J–O theory. The ion sites exhibit less asymmetry, leading to dominating covalent interactions between oxygen ligands and Sm^{3+} ions, as shown by the high value of Ω_4 compared to Ω_2 and Ω_6. We may find out more about the luminescence activators by calculating the spectroscopic quality factor using the Ω_4/Ω_6 ratio. The glasses examined show promise as luminescence activators, with computed spectroscopic quality factor values of 1.1 (SM1) and 1.5 (SM2), respectively [44,45].

Table 4. Judd–Ofelt intensity parameters (Ω_t) for fluorophosphate glasses doped with Sm^{3+} ions.

Glass ID	Ω_2 (10^{-20} cm^2)	Ω_4 (10^{-20} cm^2)	Ω_6 (10^{-20} cm^2)	σ_{rms} (10^{-6})
SM1	0.4327	1.1224	1.0071	0.354
SM2	0.9897	1.9765	1.4576	0.327

Three phenomenological spectroscopic parameters were calculated. In addition, the value of fitting quality (σ_{rms}) esti mated from the root mean square (RMS) deviation [46] was determined and is presented in Table 4. This value implies a good match between the measured P_{exp} and the calculated P_{cal} oscillator strengths.

The radiative transition probability (W_r) and the total radiative lifetime ($\tau_{rad} = 1/W_r$) of the emission level $^4G_{5/2}$ were estimated using the J-O parameters determined. In the conventional J-O approach, the Ω_t parameter values are derived using an averaging process that takes into account all the absorption bands, known as the least-squares method. The samples' observed lifetimes of the excited state $^4G_{5/2}$ (Figure 8a,b) were considerably lower than the expected radiation equivalent of τrad (refer to Table 5) and those predicted by the following relationship [42]:

$$\eta = \frac{\tau_{exp}}{\tau_{rad}} \times 100\% \quad (2)$$

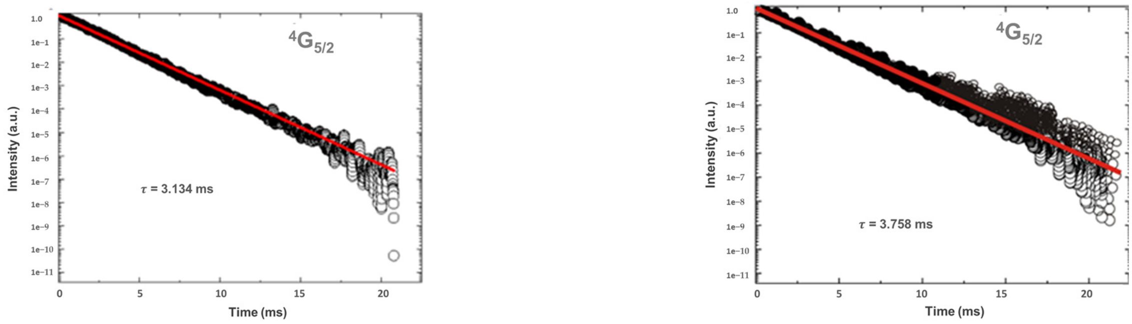

(**a**) (**b**)

Figure 8. (**a**) Luminescence lifetimes of the $^4G_{5/2}$ state of Sm^{3+} ions for sample SM1. (**b**) Luminescence lifetimes of the $^4G_{5/2}$ state of Sm^{3+} ions for sample SM2.

Table 5. This study compares the experimentally obtained lifetimes of the $^4G_{5/2}$ emission band in fluorophosphate glasses (τ_{exp}) with the lifetimes estimated using the J-O methods (τ_{rad} $^{J\text{-}O}$) and quantum efficiencies (η).

Glass ID	$^4G_{5/2}$ Lifetime (ms)		
	τ_{exp}	τ_{rad} $^{J\text{-}O}$	η (%)
SM1	3.134	3.856	96
SM2	3.758	4.865	97

This gives more than 96% of the quantum efficiency of the excited state for the material under study.

In the case of samples SM1 and SM2, one deals with high-concentration Sm^{3+} ions, leading to effective cross-relaxation (CR) between them [47]. The CR mechanism causes a decrease in the Sm^{3+}:$^4G_{5/2}$ lifetime for SM1 to 3.134 ms when compared to the J-O radiative lifetime of 3.856 ms; for sample SM2, the lifetime decreases to τ_{exp} = 3.758 ms, compared to a radiative lifetime of 4.865 ms.

3.4. Emission Spectra

The photoluminescence (PL) emission spectra of Sm^{3+}-doped fluorophosphate glasses are shown in Figure 9c, with images of the glass emission presented in Figure 9a,b.

Figure 9c displays the photoluminescence spectra produced by the glasses stimulated at 402 nm. The emission bands seen at 561.5 nm, 597.5 nm, 643.5 nm, and 708 nm, respectively, are caused by the $^4G_{5/2} \rightarrow {}^6H_{5/2}$, $^4G_{5/2} \rightarrow {}^6H_{7/2}$, $^4G_{5/2} \rightarrow {}^6H_{9/2}$, and $^4G_{5/2} \rightarrow {}^6H_{11/2}$ transitions of Sm^{3+}. The strength of the green and reddish-orange emission bands is significantly affected by the kind of glass host. $^4G_{5/2} \rightarrow {}^6H_{7/2}$ and $^4G_{5/2} \rightarrow {}^6H_{9/2}$ (red/orange) are the two distinct transition peaks of the Sm^{3+} ions in the visible emission spectrum. A decrease in the higher energy levels of $^4G_{5/2}$ may occur when higher sub-levels of energy are near a Sm^{3+} ion in the ground state because the energy can be absorbed by the Sm^{3+} ion.

The glasses tested, like glasses in other research, show that the exceptional intensity of the $^4G_{5/2} \rightarrow {}^6H_{7/2}$ transition makes them ideal for various applications, including color displays, high-density optical storage devices, and medical diagnostics. Our data closely align with those on other glasses described in the referenced studies [48–50].

(**a**)

(**b**)

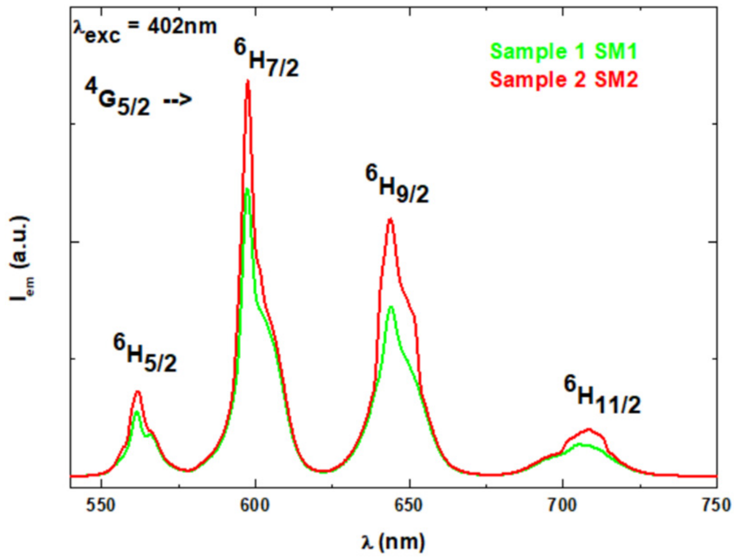

(**c**)

Figure 9. (**a**,**b**) Photos of glass emissions; (**c**) emission spectra of the glasses doped with Sm^{3+} recorded at room temperature upon 402 nm excitation.

Figure 10 shows a simplified diagram of the emission energy of Sm^{3+}. From SM1 and SM2, it can be seen that as the Sm^{3+} ions are pumped with a 402 nm excitation wavelength, they are excited to the $^6P_{3/2}$ level, and then some of the Sm^{3+} ions relax non-radioactively into lower levels of $^4G_{5/2}$ and $^4F_{3/2}$ and then decay into $^6H_{9/2}$.

Figure 11 displays a CIE 1931 chromaticity diagram, which illustrates the effect of the emission transitions at a 402 nm excitation wavelength. For the manufactured glasses SM1 and SM2, the color coordinates (x, y) are (0.551, 0.352) and (0.581, 0.398), respectively. Thus, the glasses produced in this study have the potential to serve as materials for optical gain in orange/red laser applications.

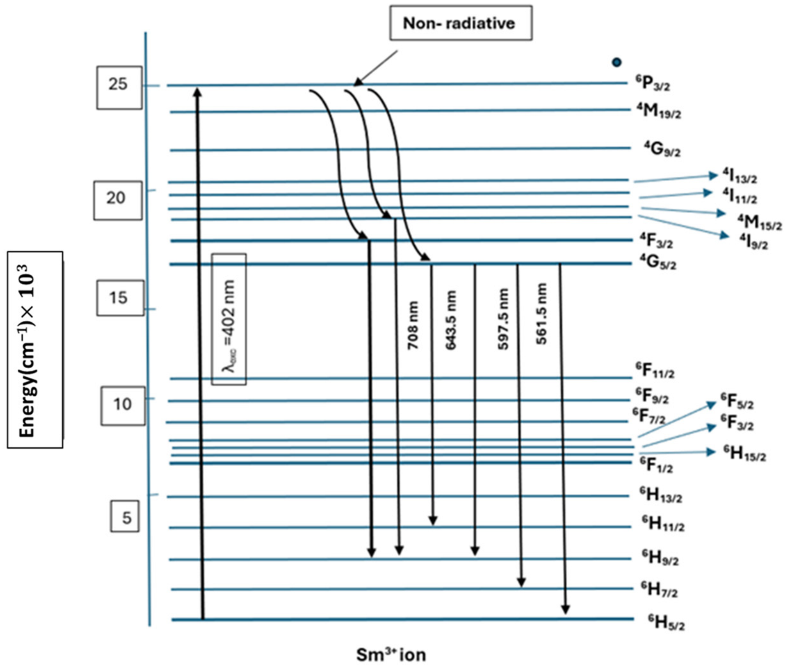

Figure 10. Schematic energy level diagram of Sm^{3+} ion shows ground state absorption and excited state absorption mechanisms.

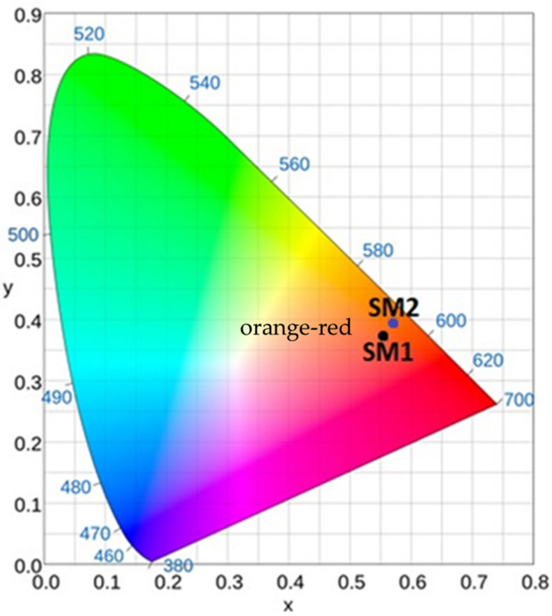

Figure 11. The CIE 1931 chromaticity diagram for the SM1 and SM2 glasses under an excitation wavelength of 402 nm.

4. Conclusions

In this study, glasses with a base chemical composition of $40P_2O_5$–30ZnO–20LiCl–$10BaF_2$ doped with Sm^{3+} were successfully prepared using a melt quenching technique. The glasses obtained fulfil the criteria to be considered superior materials for channel waveguide applications. They are compositionally and structurally homogeneous to prevent scattering and ensure consistent guiding properties and are free from significant defects and impurities that could introduce additional loss or alter the refractive index profile. From the DCS curve profiles, the glass transition temperature (T_g), the onset of the glass crystallization peak (T_x), the maximum glass crystallization peak (T_c), glass melting temperature (T_m), and thermal stability parameters were analyzed. The range of the vitreous state transition ($T_{g-endset} - T_{g-onset}$) was observed to decrease, while the glass transition temperature shifted towards higher temperatures with an increase in the Sm^{3+} ion concentration. The values of the thermal stability parameters calculated (K_w, K_H, K_{LL}) increased with a greater Sm^{3+} content, confirming the higher thermal stability of glass against devitrification on heating. Based on thermal studies, we confirmed very good glass stability. The glasses under investigation showed normal refractive index values for fluorophosphate glasses, according to ellipsometric measurements, and the Sellmeier model provided an excellent description of this index's dependency on wavelength. The Judd–Ofelt parameters calculated for the $40P_2O_5$–30ZnO–20LiCl–$10BaF_2$ glasses are as follows: SM1 ($\Omega_2 = 0.4327 \times 10^{-20}$ cm^2, $\Omega_4 = 1.1224 \times 10^{-20}$ cm^2, $\Omega_6 = 1.0071 \times 10^{-20}$ cm^2) and SM2 ($\Omega_2 = 0.9897 \times 10^{-20}$ cm^2, $\Omega_4 = 1.9765 \times 10^{-20}$ cm^2, $\Omega_6 = 1.4576 \times 10^{-20}$ cm^2). The large quantum efficiency of Sm^{3+}/SM1/$^4G_{5/2}$ (96%) and SM2 (97%) was reported for all samples. The absorption cross-section data for the $^4G_{5/2}$ – $^6H_{7/2}$ transition were determined. The CIE chromaticity coordinate (x,y) values corresponded to the orange-red region at the concentrations studied. The prominent transition peaks of the Sm^{3+} ions in the visible emission spectrum wavelength (red/orange) make our glasses useful as laser fiber sources that could be used in photodynamic therapy (PDT) treatment.

Author Contributions: B.B.-G.: conceptualization; methodology; investigation; writing—original draft; formal analysis; writing—review and editing. J.C.: conceptualization; methodology; investigation; validation. R.L.: conceptualization; methodology; investigation; writing—original draft; formal analysis; writing—review and editing. K.J.K.: conceptualization; methodology; investigation; writing—original draft; writing—review and editing. B.J.: conceptualization; methodology; investigation; writing—original draft. N.N.: formal analysis; investigation; writing—original draft; writing—review and editing; visualization. M.R.: investigation; writing—original draft; conceptualization; methodology; investigation; visualization. A.M.A.: methodology; writing—review and editing. K.I.H.: methodology; writing—original draft; visualization; writing—review and editing; funding acquisition. E.S.Y.: methodology; investigation; visualization; writing—review and editing. All authors have read and agreed to the published version of the manuscript.

Funding: This research was funded by the Ministry of Education in the KSA through project number KKU-IFP2-DA-6.

Data Availability Statement: Data are contained within the article.

Acknowledgments: The authors extend their appreciation to the Ministry of Education in the KSA for funding this research work through project number KKU-IFP2-DA-6.

Conflicts of Interest: The authors declare no conflicts of interest.

References

1. Silva, G.H.; Anjos, V.; Bell, M.J.V.; Carmo, A.P.; Pinheiro, A.S.; Dantas, N.O. Eu^{3+} emission in phosphate glasses with high UV transparency. *Lumin J.* **2014**, *154*, 294–297. [CrossRef]
2. Ravi Babu, Y.N.C.; Sree Ram Naik, P.; Vijaya Kumar, K.; Rajesh Kumar, N.; Suresh Kumar, A. Spectral investigations of Sm^{3+} doped lead bismuth magnesium borophosphate glasses. *J. Quant. Spectrosc. Radiat. Transf.* **2012**, *113*, 1669–1675. [CrossRef]
3. Jayachandiran, M.; Masilla Moses Kennedy, S. Synthesis and optical properties of Ba_3Bi_2 $(PO_4)_4$: Dy^{3+} phosphors for white light emitting diodes. *J. Alloys Compd.* **2019**, *775*, 353–359. [CrossRef]
4. Annapurna, K.; Das, M.; Kundu, M.; Dwivendhi, R.N.; Budduhudu, S. Spectral properties of Eu^{3+}: ZnO-B_2O_3-SiO_2. *J. Mol. Struct.* **2005**, *741*, 53–60. [CrossRef]
5. Bayoudhi, D.; Bouzidi, C.; Matei, E.; Secu, M.; Galca, A.C. Optical characterization of Sm^{3+} doped phosphate glasses for potential orange laser applications. *J. Lumin.* **2024**, *265*, 120204. [CrossRef]
6. Rao, C.S.; Jayasankar, C.K. Spectroscopic and radiative properties of Sm^{3+}-doped K–Mg–Al phosphate glasses. *Opt. Commum.* **2013**, *286*, 204–210. [CrossRef]
7. Kesavulu, C.R.; Jayasankar, C.K. Spectroscopic properties of Sm^{3+} ions in lead fluorophosphate glasses. *J. Lumin.* **2012**, *132*, 2802–2809. [CrossRef]
8. Mahato, K.K.; Rai, D.K.; Rasi, S.B. Optical studies of Sm^{3+} doped oxyfluoroborate glass. *Solid State Commun.* **1998**, *108*, 671–676. [CrossRef]

9. Swapna, K.; Mahamuda, S.; Srinivasa Rao, A.; Sasikala, T.; Rama Moorthy, L. Visible luminescnence characteristics of Sm^{3+} doped zinc alumino bismuth borate glasses. *J. Lumin.* **2014**, *146*, 288–294. [CrossRef]
10. Souza Filho, A.G.; Mendes Filho, J.; Melo, F.E.A.; Custodio, M.C.C.; Lebullenger, R.; Hern, A.C. Optical properties of Sm^{3+} doped lead fluoroborate glasses. *J. Phys. Chem. Solids* **2000**, *61*, 1535–1542. [CrossRef]
11. Pan, C.; Kou, K.; Wu, G.; Zhang, Y.; Wang, Y. Fabrication and characterization of AlN/PTFE composites with low dielectric constant and high thermal stability for electronic packaging. *J. Mater. Sci. Mater. Electron.* **2016**, *27*, 286–292. [CrossRef]
12. Okasha, A.; Gaafar, M.S.; Marzouk, S.Y. The influence of concentration variationon the spectroscopic behavior of Sm^{3+} doped zinc–lead-phosphates glasses for orange and reddishorangelight-emitting applications: Experimental and Judd–Ofelt approach. *J. Mater. Sci. Mater. Electron.* **2023**, *34*, 354. [CrossRef]
13. Hussain, S.; Amjad, R.J.; Tanveer, M.; Nadeem, M.; Mahmood, H.; Sattar, A.; Iqbal, A.; Hussain, I.; Amjad, Z.; Hussain, S.Z.; et al. Optical Investigation of Sm^{3+} Doped in Phosphate Glass. *Glass Phys. Chem.* **2017**, *43*, 538–547. [CrossRef]
14. Marzouk, M.A.; Elbatal, H.A. Investigation of photoluminescence and spectroscopic properties of Sm^{3+}-doped heavy phosphate glasses before and after gamma irradiation. *Appl. Phys. A* **2021**, *127*, 70. [CrossRef]
15. Alzahrani, J.S.; Alrowaili, Z.A.; Alqahtani, M.S.; Eke, C.; Olarinoye, I.O.; Adam, M.; Al-Buriahi, M.S. Influence of Alkaline Earth Metals on the Optical Properties and Radiation-Shielding Effectiveness of Sm^{3+}-Doped Zinc Borophosphate Glasses. *J. Electron. Mater.* **2023**, *52*, 7794–7806. [CrossRef]
16. Okasha, A.; Abdelghany, A.M.; Mohamed, S.K.; Marzouk, S.Y.; El-Batal, H.A.; Gaafar, M.S. Gamma ray interactions with samarium doped strontium phosphate glasses. *J. Mater. Sci. Mater. Electron.* **2018**, *29*, 20907–20913. [CrossRef]
17. Vahedi, S.; Okada, G.; Koughia, C.; Sammynaiken, R.; Edgar, A.; Kasap, S. ESR study of samarium doped fluorophosphate glasses for high-dose, high-resolution dosimetry. *Opt. Mater. Express* **2014**, *4*, 1244–1256. [CrossRef]
18. Hamdy, Y.M.; Bahammam, S.; Abd El All, S.; Ezz-Eldin, F.M. Spectroscopic properties and luminescence behavior of γ irradiated Sm^{3+} doped oxy-fluoride phosphate glasses. *Results Phys.* **2017**, *7*, 1223–1229. [CrossRef]
19. Ahmed, R.M.; Taha, T.A.; Ezz-Eldin, F.M. Investigation of Sm_2O_3 effect on opto-electrical parameters and dielectric properties of some fluorophosphate glasses. *J. Mater. Sci. Mater. Electron.* **2021**, *32*, 28919–28934. [CrossRef]
20. Mrabet, H.; Khattech, I.; Bouzidi, S.; Kechiche, L.; Jbeli, A.; Al Harbi, N.; Bouzidi, C.; Muñoz, F.; Balda, R. Influence of barium substitution on the physical, thermal, optical and luminescence properties of Sm^{3+} doped metaphosphate glasses for reddish orange light applications. *RSC Adv.* **2024**, *14*, 2070–2079. [CrossRef]
21. Chicilo, F.; Okada, G.; Belev, G.; Chapman, D.; Edgar, A.; Curry, R.J.; Kasap, S. Instrumentation for high-dose, high resolution dosimetry for microbeam radiation therapy using samarium-doped fluoroaluminate and fluorophosphate glass plates. *Meas. Sci. Technol.* **2019**, *65*, 075010. [CrossRef]
22. Brancaleon, L.; Moseley, H. Laser and non-laser light sources for photodynamic therapy. *Lasers Med. Sci.* **2002**, *17*, 173–186. [CrossRef] [PubMed]
23. Brown, S.B. Photodynamic therapy: Two photons are better than one. *Nat. Photonics* **2008**, *2*, 394–395. [CrossRef]
24. Kim, M.M.; Darafsheh, A. Light Sources and Dosimetry Techniques for Photodynamic Therapy. *Photochem. Photobiol.* **2020**, *96*, 280–294. [CrossRef] [PubMed]
25. Shafirstein, G.; Bellnier, D.; Oakley, E.; Hamilton, S.; Potasek, M.; Beeson, K.; Parilov, E. Interstitial photodynamic therapy—A focused review. *Cancers* **2017**, *9*, 12. [CrossRef]
26. Burtan, B.; Reben, M.; Cisowski, J.; Wasylak, J.; Nosidlak, N.; Jaglarz, J.; Jarząbek, B. Influence of Rare Earth Ions on the Optical Properties of Tellurite Glass. *Acta Phys. Polon. A* **2011**, *120*, 579–581. [CrossRef]
27. Burtan, B.; Mazurak, Z.; Cisowski, J.; Czaja, M.; Lisiecki, R.; Ryba-Rymanowski, W.; Reben, M.; Wasylak, J. Optical properties of Nd^{3+} and Er^{3+} ions in TeO_2–WO_3–PbO–La_2O_3 glasses. *Opt. Mater.* **2012**, *34*, 2050–2054. [CrossRef]
28. Burtan, B.; Cisowski, J.; Mazurak, Z.; Jarząbek, B.; Czaja, M.; Lisiecki, R.; Ryba Romanowski, W.; Reben, M.; Grelowska, I. Concentration-dependent spectroscopic properties of Pr^{3+} ions in TeO_2-WO_3-PbO-La_2O_3 glass. *J. Non-Cryst. Solids* **2014**, *400*, 21–26. [CrossRef]
29. Burtan-Gwizdala, B.; Reben, M.; Cisowski, J.; Lisiecki, R.; Ryba-Romanowski, W.; Jarzabek, B.; Mazurak, Z.; Nosidlak, N.; Grelowska, I. The influence of Pr^{3+} content on luminescence and optical behavior of TeO_2-WO_3-PbO Lu_2O_3 glass. *Opt. Mater.* **2015**, *47*, 231–236. [CrossRef]
30. Mito, T.; Fujino, S.; Takebe, H.; Moringa, K.; Todorki, S.; Sakaguchi, S. Refractive index and material dispersions of multi-component oxide glasses. *J. Non-Cryst. Solids* **1997**, *210*, 155–162. [CrossRef]
31. Herzinger, C.M.; Johs, B.; McGahan, W.A.; Woollam, J.A.; Paulson, W. Ellipsometric determination of optical constants for silicon and thermally grown silicon dioxide via a multi-sample, multi-wavelength, multi-angle investigation. *J. Appl. Phys.* **1998**, *83*, 3323–3336. [CrossRef]
32. Hruby, A. Evaluation of glass-forming tendency by means of DTA. *Czechoslov. J. Phys.* **1972**, *22*, 1187–1193. [CrossRef]
33. Lu, Z.P.; Liu, C.T. A new glass-forming ability criterion for bulk metallic glasses. *Acta Mater.* **2002**, *50*, 3501–3512. [CrossRef]
34. Jiusti, J.; Cassar, D.R.; Zanotto, E.D. Which glass stability parameters can assess the glass-forming ability of oxide systems. *Int. J. Appl. Glass Sci.* **2020**, *11*, 612–621. [CrossRef]
35. Mawlud, S.Q.; Ameen, M.M.; Md Sahar, R.; Ahmed, K.F. Influence of Sm_2O_3 Ion Concentration on Structural and Thermal Modification of TeO_2-Na_2O Glasses. *J. Appl. Mech. Eng.* **2016**, *5*, 1000222. [CrossRef]

36. Manjeet; Kumar, A.; Anu; Lohan, R.; Deopa, N.; Kumar, A.; Chahal, R.P.; Dahiya, S.; Punia, R.; Rao, A.S. Impact of Sm^{3+} ions on structural, thermal, optical and photoluminescence properties of ZnO–Na_2O–PbO B_2O_3 glasses for optoelectronice device applications. *Opt. Mater.* **2023**, *139*, 113778. [CrossRef]
37. Elkhoshkhany, N.; Marzouk, S.Y.; Khattab, M.A.; Dessouki, S.A. Influence of Sm_2O_3 addition on Judd-Ofelt parameters, thermal and optical properties of the TeO_2-Li_2I ZnO Nb_2O_5 glass system. *Mater. Charact.* **2018**, *144*, 274–286. [CrossRef]
38. Mohan Babu, A.; Jaamalaiah, B.C.; Sasikala, T.; Saleem, S.A.; Rama Moorthy, L. Absorption and emission spectral studies of Sm^{3+}-doped lead tungstate tellurite glasses. *J. Alloys Comp.* **2011**, *509*, 4743–4747. [CrossRef]
39. Judd, B.R. Optical absorption intensities of rare-earth ions. *Phys. Rev.* **1962**, *127*, 750–761. [CrossRef]
40. Ofelt, G.S. Intensities of crystal spectra of rare-earth ions. *J. Chem. Phys.* **1962**, *37*, 511–520. [CrossRef]
41. Klimesz, B.; Lisiecki, R.; Ryba-Romanowski, W. Sm^{3+}-doped oxyfluorotellurite glasses spectroscopic, luminescence and temperature sensor properties. *J. Alloys Compd.* **2019**, *788*, 658–665. [CrossRef]
42. Aboudeif, Y.M.; Moteb Alqahtani, M.; Emara, A.M.; Reben, M.; Yousef, E.-S. Luminescence of Phosphate Glasses: P_2O_5 -ZnO-BaF_2-K_2TeO_3-Al_2O_3-Nb_2O_5 doped with Sm^{3+} ions for display and laser materials. *J. Electron. Mater.* **2020**, *49*, 4144–4153. [CrossRef]
43. Sharma, Y.K.; Surana, S.S.L.; Dubedi, R.P.; Joshi, V. Spectroscopic and radiative properties of Sm^{3+} doped zinc fluoride borophosphate glasses. *Mater. Sci. Eng. B* **2005**, *119*, 131–135. [CrossRef]
44. Shoaib, M.; Rooh, G.; Rajaramakrishna, R.; Chanthima, N.; Kim, H.J.; Tuscharoen, S.; Kaewkhao, J. Physical and luminescence properties of samarium doped oxide and oxyfluoride phosphate glasses. *Mater. Chem. Phys.* **2019**, *229*, 514–522. [CrossRef]
45. Swetha, B.N.; Keshavamurthy, K.; Pramod, A.G.; Devarajulu, G.; Roopa, K.P.; Rajeshree Patwari, D.; Kebaili, I.; Ahmed, S.B.; Sayyed, M.I.; Khan, S.; et al. Improved photoluminescence and spectroscopic features of Sm^{3+}-doped alkali borate glasses by embedding silver nanoparticles. *J. Non-Cryst. Solids* **2022**, *579*, 121371. [CrossRef]
46. Yousef, E.S.; Elokr, M.M.; Aboudeif, Y.M. Raman spectroscopy and raman gain coefficient of telluroniobium-zinc-lead oxyglasses doped with rare earth. *Chalcogenide Lett.* **2015**, *12*, 597.
47. Jlassi, I.; Mnasri, S.; Elhouichet, H. Concentration dependent spectroscopic behavior of Sm^{3+}-doped sodium fluoro-phosphates glasses for orange and reddish-orange light emitting applications. *J. Lumin.* **2018**, *199*, 516–527. [CrossRef]
48. Timoshenko, A.D.; Matvienko, O.O.; Doroshenko, A.G.; Parkhomenko, S.V.; Vorona, I.O.; Kryzhanovska, O.S.; Safronova, N.A.; Vovk, O.O.; Tolmachev, V.; Baumer, V.N.; et al. Highly-doped YAG:Sm^{3+} transparent ceramics: Effect of Sm^{3+} ions concentration. *Ceram. Int.* **2023**, *49*, 7524–7533. [CrossRef]
49. Abdullahi, T.I.; Hashim, S.; Ghoshal, S.K.; Sayyed, M.I. Tailored spectroscopic characteristics of a new type of CuO nanoparticles inserted borate glass system: Samarium concentration tuning effect. *Helyon* **2023**, *9*, 20262. [CrossRef]
50. Roopa; Eraiah, B. Impact of samarium ion concentration on the physical, structural and optical properties of multi-component borate glasses. *J. Non-Cryst. Solids* **2022**, *596*, 121866. [CrossRef]